


Cite this: *Chem. Sci.*, 2021, 12, 1551

All publication charges for this article have been paid for by the Royal Society of Chemistry

# A chemical circular communication network at the nanoscale†

Beatriz de Luis,<sup>ab</sup> Ángela Morellá-Aucejo,<sup>ab</sup> Antoni Llopis-Lorente,<sup>ab</sup> Tania M. Godoy-Reyes,<sup>ab</sup> Reynaldo Villalonga,<sup>e</sup> Elena Aznar,<sup>ab</sup> Félix Sancenón<sup>ab</sup> and Ramón Martínez-Máñez<sup>ab</sup> 

In nature, coordinated communication between different entities enables a group to accomplish sophisticated functionalities that go beyond those carried out by individual agents. The possibility of programming and developing coordinated communication networks at the nanoscale—based on the exchange of chemical messengers—may open new approaches in biomedical and communication areas. Here, a stimulus-responsive circular model of communication between three nanodevices based on enzyme-functionalized Janus Au–mesoporous silica capped nanoparticles is presented. The output in the community of nanoparticles is only observed after a hierarchically programmed flow of chemical information between the members.

Received 28th August 2020  
Accepted 29th November 2020

DOI: 10.1039/d0sc04743k

rsc.li/chemical-science

## Introduction

Chemical communication is based on the exchange of molecular messengers between different entities. In nature, living cells and organisms rely on chemical communication processes for sustaining vital biological functions.<sup>1–4</sup> For instance, organelles exchange messengers that allow cellular metabolism; neurons communicate by exchanging neurotransmitters; and physiological functions are regulated by hormone molecules segregated by distant cells. At a larger scale, insects, bacteria and pluricellular organisms communicate with peers by means of pheromones. Communication networks enable a group to share information and act together towards the achievement of a common goal.<sup>5,6</sup> Considering this aim, coordinated communication displays an essential role as it is necessary to organize the collective behaviour in a defined order to assure efficiency and productivity.<sup>7,8</sup> In fact, nature life is based on communication processes developed in coordinated communities at the molecular scale involving the use of

chemical messengers. As examples of coordinated groups, termite populations and fish shoals have chemically coordinated alarm systems in which a member detects an environment disturbance and secretes alarm molecules. Other members sense this message and expel chemical secretions, subsequently spreading alarm through the community and resulting in the articulation of a collective response (*e.g.*, release of toxic/repellent chemicals or colony recruitment).<sup>9–11</sup>

Transferring communication capabilities to human-made nanoscale systems has attracted significant attention in recent years due to potential applications in areas such as biomedicine or ICT (Information and Communication Technologies).<sup>12–16</sup> Compared to traditional telecommunication technologies, chemical communication offers interesting features such as the reduced size of molecular transceivers and receivers, minimal power consumption and the ability to operate in biological and physiological environments. Several micro- and nanocarriers capable of interacting with living systems by means of sending or receiving chemical messengers have been developed.<sup>17–23</sup> Linear communication between particles or feedback between two particles has also been reported.<sup>24,25</sup> However, the field is still in its infancy and more complex communication communities should be demonstrated with the future aim to integrate coordinated multicomponent communities of nanodevices with advanced capabilities.<sup>26–29</sup> Strategies of cooperation and coordination between different nanoparticles may enable sophisticated functionalities that go beyond those carried out by individual agents. However, regardless of the aforementioned advancements made in the last years, the definition of technologies to support practical and useful applications of communication at nanoscale, while essential to motivate further growth of this field in the research community, is still very limited and still scarcely explored.

<sup>a</sup>Instituto Interuniversitario de Investigación de Reconocimiento Molecular y Desarrollo Tecnológico (IDM), Universitat Politècnica de València, Universitat de València, Camino de Vera s/n, 46022 Valencia, Spain. E-mail: rmaez@gim.upv.es

<sup>b</sup>CIBER de Bioingeniería, Biomateriales y Nanomedicina (CIBER-BBN), Spain

<sup>c</sup>Unidad Mixta UPV-CIPF de Investigación en Mecanismos de Enfermedades y Nanomedicina, Universitat Politècnica de València, Centro de Investigación Príncipe Felipe, Valencia, Spain

<sup>d</sup>Unidad Mixta de Investigación en Nanomedicina y Sensores, Universitat Politècnica de València, Instituto de Investigación Sanitaria La Fe, Valencia, Spain

<sup>e</sup>Nanosensors & Nanomachines Group, Department of Analytical Chemistry, Faculty of Chemistry, Complutense University of Madrid, Madrid, Spain

† Electronic supplementary information (ESI) available: Chemicals, general methods, characterization, procedures and additional figures. See DOI: 10.1039/d0sc04743k

In this scenario, we report herein a circular model of a multicomponent communication network of nanoparticles based on the exchange of chemical messages. Today it is well recognized the ubiquity of cyclic organization in biology as it provides invaluable resources for controlling and orchestrating biological operations, giving rise to complex temporal dynamics in nature.<sup>30</sup> For instance, dynamical feedback is observed in biological reaction networks where metabolic processes regulate their activity or resupply the initial substrate in a cyclic manner. Our communication system consists of three enzyme-functionalized Janus Au-mesoporous silica nanoparticles (Au-**MSNPs**) which display a double receiver-sender behaviour,<sup>31,32</sup> as depicted in Fig. 1A. The mesoporous face of nanodevice **1** (**S1<sub>βgal</sub>**) is loaded with the fluorescent dye [Ru(bpy)<sub>3</sub>]Cl<sub>2</sub> and capped with disulfide-containing oligo(ethylene glycol) chains (PEG) acting as gatekeepers, whereas the enzyme β-galactosidase (βgal) is attached to the gold face. In nanoparticle **2** (**S2<sub>galox</sub>**), the enzyme galactose oxidase (galox) is immobilized on

the Au face, while the mesoporous silica is loaded with methyl 4-(bromomethyl)benzoate and the mesopores capped with a H<sub>2</sub>O<sub>2</sub>-sensitive self-immolative arylboronate derivative (**1**) which forms a host-guest complex with  $\beta$ -cyclodextrin (Fig. 1B).<sup>33</sup> Finally, the nanodevice **3** (**S3<sub>est</sub>**) is functionalized with the enzyme esterase on the Au face, loaded with the reductive species tris(2-carboxyethyl)phosphine hydrochloride (TCEP) in the mesoporous face and capped with a pH responsive supramolecular nanovalve consisting of an inclusion complex between a benzimidazole moiety and  $\beta$ -cyclodextrin.<sup>34</sup>

As illustrated in Fig. 1A, this circular communication is triggered in the presence of lactose (input). Lactose is transformed into galactose by the enzyme  $\beta$ -galactosidase attached to the gold face of **S1**<sub>gal</sub>. Galactose acts as a chemical messenger that is transmitted and sensed by galactose oxidase enzyme on **S2**<sub>galox</sub> resulting in the formation of galacto-hexodialdose and H<sub>2</sub>O<sub>2</sub>. Hydrogen peroxide triggers the self-immolative cleavage<sup>33</sup> of the gatekeeper on **S2**<sub>galox</sub> allowing the delivery of a benzoate

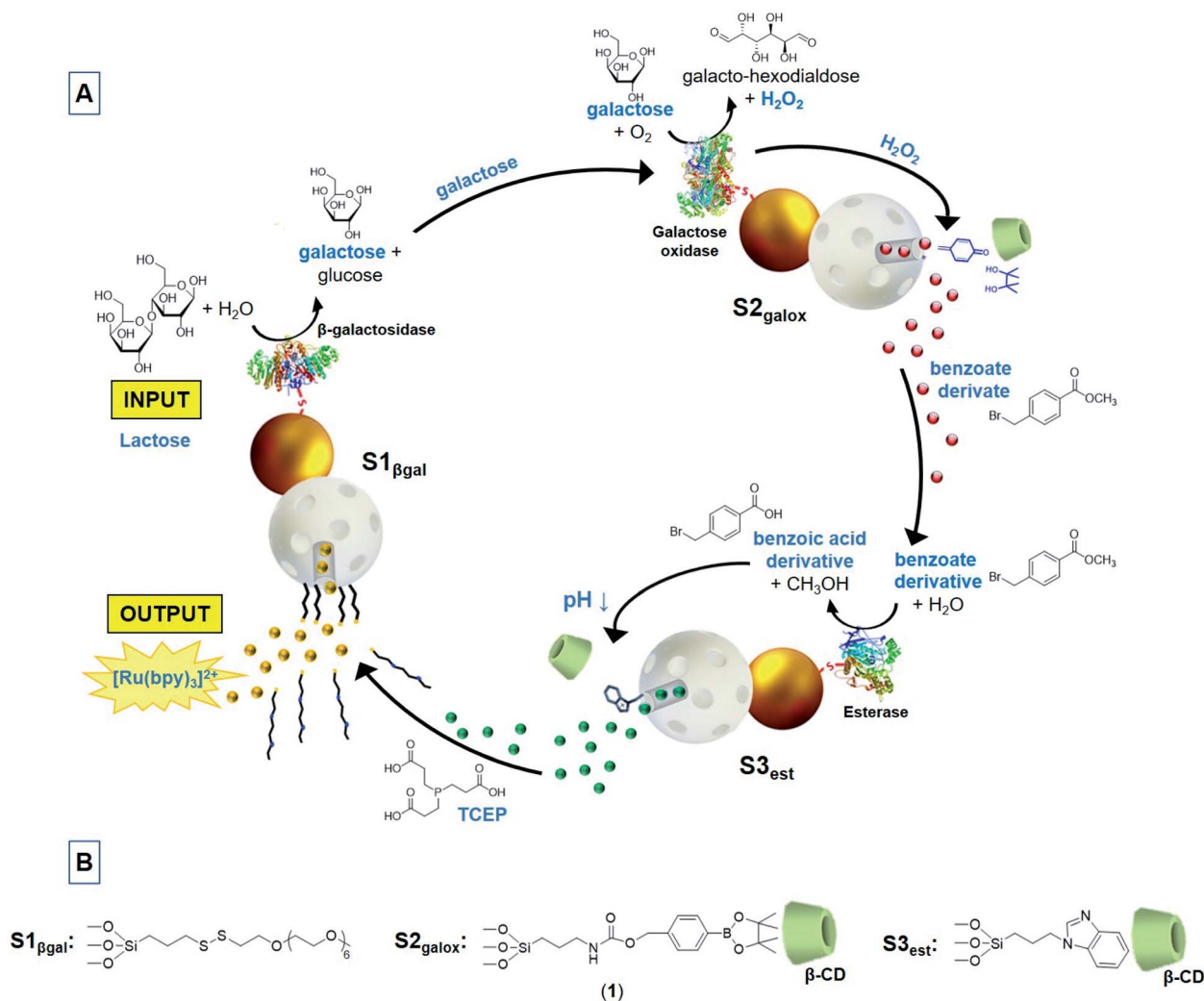


**Fig. 1** (A) Representation of the circular model of communication between three enzyme-functionalized Janus Au–mesoporous silica capped nanoparticles based on the programmed exchange of chemical messengers. (B) Representation of the molecular gatekeepers of each nano-device. From left to right: disulfide-linked PEG chain, self-immolative arylboronate derivative (**1**)- $\beta$ -cyclodextrin inclusion complex and benzimidazole- $\beta$ -cyclodextrin inclusion complex.

derivative (methyl 4-(bromomethyl)benzoate) as a second chemical messenger that is detected by the enzyme esterase on **S3<sub>est</sub>** and transformed into the corresponding benzoic acid derivative. Formation of benzoic acid induces a local drop of the pH causing the protonation of benzimidazole moieties,<sup>35</sup> dethreading of the nanovalve and the delivery of the reductive agent (TCEP) from **S3<sub>est</sub>**. TCEP acts as a third chemical messenger that closes the loop by communicating **S3<sub>est</sub>** with **S1<sub>βgal</sub>**, as it produces the reductive cleavage of the disulfide bonds of the oligo(ethylene glycol) chains anchored to the mesoporous face of **S1<sub>βgal</sub>**. Eventually, the subsequent release of the dye [Ru(bpy)<sub>3</sub>]Cl<sub>2</sub> from **S1<sub>βgal</sub>** is produced as the output collective response of the communication network.

## Results and discussion

### Preparation and characterization of the nanodevices

Janus Au-**MSNPs** were prepared using gold nanoparticles (of *ca.* 20 nm obtained by reduction of HAuCl<sub>4</sub>·3H<sub>2</sub>O with sodium citrate) and **MSNPs** (of *ca.* 100 nm MCM-41-type nanoparticles obtained by an alkaline hydrolysis reaction), as adapted from a previous study.<sup>31</sup> **MSNPs** were partially imbedded at the interface of a Pickering emulsion, formed by paraffin wax (oily phase) and water-ethanol (aqueous phase). The un-masked **MSNPs** surface was decorated with reactive thiol groups, by reaction with (3-mercaptopropyl)trimethoxysilane, on which citrate-capped Au nanoparticles were subsequently attached. After removing the paraffin with chloroform, the starting Janus Au-**MSNPs** (**S0**) were obtained. **S1** was prepared loading **S0** with the [Ru(bpy)<sub>3</sub>]Cl<sub>2</sub>·6H<sub>2</sub>O dye and protecting the Au face with 3-mercaptopropionic acid. The resulting solid was reacted with (3-mercaptopropyl)trimethoxysilane, with 2,2'-dipyridyl disulfide and then with O-(2-mercaptoethyl)-O'-methyl-hexa(ethylene glycol) to give the final capped Janus nanoparticles **S1**. **S1<sub>βgal</sub>** was obtained from **S1** by anchoring β-galactosidase on the carboxylate-modified Au face by means of well-known cross-linking EDC/NHS chemistry resulting in the coupling between the free amino groups of lysine residues from the enzyme and the activated Au carboxyl groups.<sup>36</sup> **S2** was prepared loading **S0** with methyl 4-(bromomethyl)benzoate and adding 3-mercaptopropionic acid to functionalize the gold face. The mesoporous face was reacted with the self-immolative molecule (**1**) (Fig. 1B) and the system was capped by the formation of an inclusion complex between (**1**) and β-cyclodextrin (formation constant = 31.1 ± 0.7 M<sup>-1</sup>).<sup>37</sup> For the preparation of **S2<sub>galox</sub>**, galactose oxidase was anchored on the Au face of **S2** following a similar procedure as previously described for **S1<sub>βgal</sub>**. **S3** was prepared by reacting the mesoporous face of **S0** with (3-iodopropyl)trimethoxysilane and then with benzimidazole. The resulting solid was treated with 3-mercaptopropionic acid, loaded with tris(2-carboxyethyl)phosphine and capped with β-cyclodextrin as it threads onto benzimidazole forming an inclusion complex (formation constant = 104 ± 8 M<sup>-1</sup>).<sup>34</sup> **S3<sub>est</sub>** was obtained anchoring the esterase enzyme on the Au face of **S3** following the above described EDC/NHS chemistry methodology. As control solids, **S2<sub>blank</sub>** and **S3<sub>blank</sub>** were prepared following the

same procedure described for **S2<sub>galox</sub>** and **S3<sub>est</sub>** respectively but in this case the mesoporous container was not loaded.

The nanoparticles were characterized using standard techniques (Fig. 2, for more details see ESI†). Powder X-ray diffraction patterns at low (1.5 < 2θ < 7) and at high angles (35 < 2θ < 80) of different prepared nanoparticles showed in all cases low-angle reflections of mesoporous silica and high-angle cubic gold characteristic diffraction peaks (see also Fig. S3†). UV/vis of the synthesized Au nanoparticles showed a single surface plasmon absorption band at 524 nm, characteristic of spherically shaped nanospheres with approximately 20 nm diameter that was redshifted to 533 nm in **S0** (Fig. S4†). The presence of the mesoporous structure as well as Au nanoparticles was confirmed by transmission electron microscopy (TEM) (Fig. 2B, additional images in Fig. S2†), obtaining similar Au-**MSNPs** ratios as previously reported.<sup>38</sup> N<sub>2</sub> adsorption-desorption isotherms of the calcined **MSNPs** and Janus Au-**MS** nanoparticles **S0** showed an adsorption step at intermediate *P/P<sub>0</sub>* value 0.3 (Fig. S5†), which is characteristic for mesoporous solids with empty pores. Application of the BET model resulted in a value for the total specific surface of 1079 m<sup>2</sup> g<sup>-1</sup> for calcined **MSNPs** and 802 m<sup>2</sup> g<sup>-1</sup> for **S0**. Pore sizes and total pore volumes were calculated with the BJH model (Table S1†). The hydrodynamic size and zeta potential of different solids were measured by dynamic light scattering (DLS) (Fig. 2C and Table S2†). **S0** showed a hydrodynamic diameter of 115 ± 4 nm that increased to 133 ± 18 nm, 143 ± 15 nm and 148 ± 18 nm for **S1<sub>βgal</sub>**, **S2<sub>galox</sub>** and **S3<sub>est</sub>** respectively, whereas Z potential of **S0** was -28.4 ± 0.5 and -31.3 ± 0.9, -26.3 ± 0.4 and -30.4 ± 0.7 for **S1<sub>βgal</sub>**, **S2<sub>galox</sub>** and **S3<sub>est</sub>**. From elemental analysis and delivery studies the amounts of different components on the nanoparticles were calculated (Table S3†). The presence of β-galactosidase, galactose oxidase and esterase enzymes on **S1<sub>βgal</sub>**, **S2<sub>galox</sub>** and **S3<sub>est</sub>** was confirmed by enzyme activity assays (Fig. S6–S8, see ESI† for details) revealing activities of 0.001 U, 0.124 U and 0.165 U per mg of solid, respectively. TEM-EDX mapping of the final nanodevices **S1<sub>βgal</sub>**, **S2<sub>galox</sub>** and **S3<sub>est</sub>** confirmed the presence of the expected atoms in the solids. Images showed that gold surfaces were rich in sulfur atoms, strongly suggesting the preferential localization of the enzymes in the Au face (Fig. 2D, S9–S11†) as they were immobilized by means of 3-mercaptopropionic acid. Moreover, the remarkable presence of sulfur atoms in the whole scaffold **S1<sub>βgal</sub>** is attributed to the disulfide bonds of the gatekeeper PEG in the mesoporous face. In turn, the slight signal of sulfur atoms in **S2<sub>galox</sub>** and **S3<sub>est</sub>** is attributed to the (3-mercaptopropyl)trimethoxysilane employed to attach the gold nanoparticles to the silica container during the scaffold synthesis. Boron atoms and nitrogen atoms in **S2<sub>galox</sub>** are ascribed to the boronic esters and carbamate groups of the gatekeepers in **S2<sub>galox</sub>**, whereas the abundance of nitrogen atoms in **S3<sub>est</sub>** is due to the presence of benzimidazole moieties.

### Release studies

**Individual studies.** In a first step, we tested the ability of **S1<sub>βgal</sub>**, **S2<sub>galox</sub>** and **S3<sub>est</sub>** nanodevices to recognize the



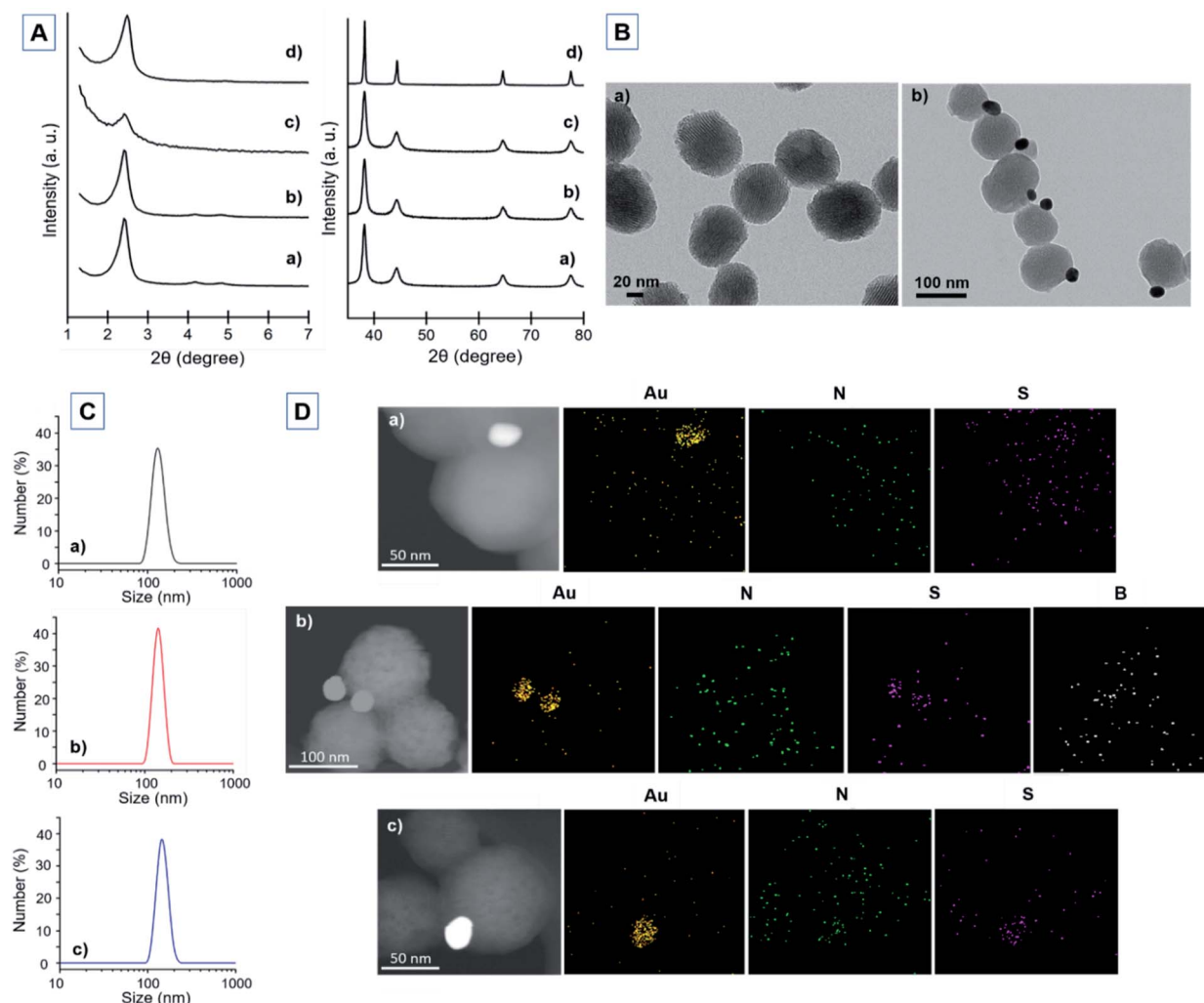


Fig. 2 (A) Powder X-ray diffraction patterns of the solids (a) Janus Au–MS nanoparticles **S0**, (b) solid **S1**, (c) solid **S2** and (d) solid **S3** at low (left) and high (right) angles. (B) Representative TEM images of (a) calcined MSNPs and (b) Janus Au–MS nanoparticles **S0**. (C) Hydrodynamic diameter distribution (nm) determined by DLS for the final enzyme-functionalized nanodevices: (a) **S1**<sub>βgal</sub> ( $133 \pm 18$  nm), (b) **S2**<sub>galox</sub> ( $143 \pm 15$  nm) and (c) **S3**<sub>est</sub> ( $148 \pm 18$  nm). (D) TEM-EDX element mapping of the nanodevice (a) **S1**<sub>βgal</sub>, (b) **S2**<sub>galox</sub> and (c) **S3**<sub>est</sub>.

corresponding input and subsequently deliver their payload. For this, we prepared [Ru(bpy)<sub>3</sub>]Cl<sub>2</sub> (dye) loaded nanoparticles (**S1**<sub>βgal</sub>, **S2**<sub>galox-dye</sub> and **S3**<sub>est-dye</sub>) and monitored dye release in shaken aqueous solutions at pH 7.5 (20 mM sodium sulfate) in the absence and in the presence of the corresponding input (TCEP for **S1**<sub>βgal</sub>, galactose for **S2**<sub>galox-dye</sub> and methyl 4-(bromomethyl)benzoate for **S3**<sub>est-dye</sub>). Aliquots were taken at scheduled times, centrifuged to remove nanoparticles, and the fluorescent emission band of [Ru(bpy)<sub>3</sub>]Cl<sub>2</sub> was measured at 595 nm ( $\lambda_{\text{exc}} = 453$  nm). Individual delivery studies revealed payload release in the presence of the corresponding stimulus while imperceptible or very low dye delivery was observed in its absence (Fig. 3). Moreover, several release control experiments were carried out for each nanodevice employing their own chemical trigger as input (positive controls) and the chemical trigger of the other nanocarriers (negative controls) revealing no potential interferences between them (Fig. S12–S14 in ESI†). It was also proved that the presence of the corresponding enzyme in **S2**<sub>galox-dye</sub> and **S3**<sub>est-dye</sub> was necessary to achieve the

nanodevice gate opening and the subsequent cargo release (Fig. S13 and S14 in ESI†).

**Linear communication between pairs of nanoparticles.** Afterwards, in a further step to evaluate the feasibility of the communication network, we tested the linear communication between each pair of nanodevices [1–2 (**S1**<sub>βgal</sub>/**S2**<sub>galox-dye</sub>), 2–3 (**S2**<sub>galox</sub>/**S3**<sub>est-dye</sub>), 3–1 (**S3**<sub>est</sub>/**S1**<sub>βgal</sub>)]. For doing so, each pair was placed in solution and shaken in the absence and in the presence of the communication activating molecule (*i.e.* lactose for 1–2, galactose for 2–3, and methyl 4-(bromomethyl)benzoate for 3–1). The corresponding nanoparticle concentration conditions were adjusted considering the activity of immobilized enzymes and the solubility of methyl 4-(bromomethyl)benzoate. As shown in Fig. 4, in the three cases a remarkable output (dye delivery) was observed in the presence of the corresponding chemical trigger while a low signal (dye delivery below 20%) was found in its absence. Besides, we confirmed the inability of lactose input to disrupt the disulfide bonds of the molecular gate on nanoparticle 1 (**S1**<sub>βgal</sub>) (Fig. S12†) demonstrating that





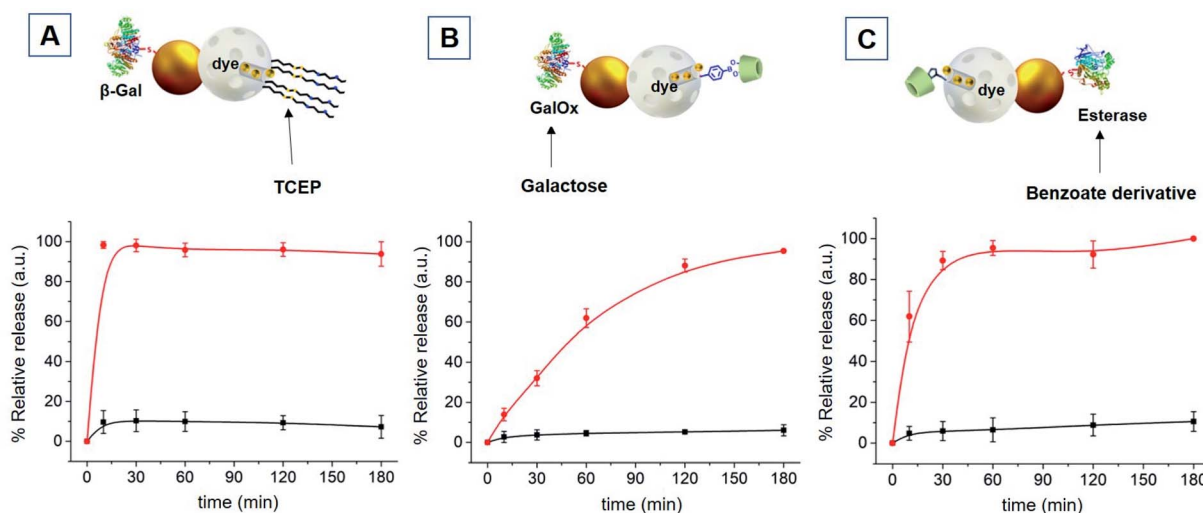


Fig. 3 Schemes of the individual experiments and normalized cargo release kinetics from (A)  $S1_{\beta gal}$ , (B)  $S2_{gal ox}$ -dye and (C)  $S3_{est}$ -dye in the absence (black curves) and in the presence (red curves) of the corresponding input (TCEP at 1 mM, galactose at 50 mM and methyl 4-(bromomethyl)benzoate at 1 mM final concentration, respectively). Error bars correspond to the s.d. from three independent experiments.

communication between pair 1–2 relied exclusively on the generation of messenger 1 (galactose) by  $\beta$ -galactosidase. All these experiments verified the establishment of linear communication pathways and successful exchange of chemical messages between pairs of nanodevices.

**Circular communication.** Finally, we tested the realization of the whole circular pattern of communication (Fig. 1A). For these experiments, the three nanodevices ( $S1_{\beta gal}$ ,  $S2_{gal ox}$  and  $S3_{est}$ ) were brought together in aqueous solution (20 mM sodium sulfate, pH 7.5) in the same reaction vessel and divided in two

fractions. After one hour of incubation, either water (for blank) or lactose 50 mM were added. Aliquots were taken at scheduled times, centrifuged to remove nanoparticles, and the emission at 595 nm of  $[Ru(bpy)_3]Cl_2$  was measured. As depicted in Fig. 5, there was a continuous steady delivery of the cargo from  $S1_{\beta gal}$  in the presence of lactose. In contrast, delivery of less than 20% of the maximum delivery observed was found for the community of nanoparticles in the absence of the communication triggering molecule. From 10 hours ahead, the blank fraction (no input) stabilized whereas in the lactose fraction delivery

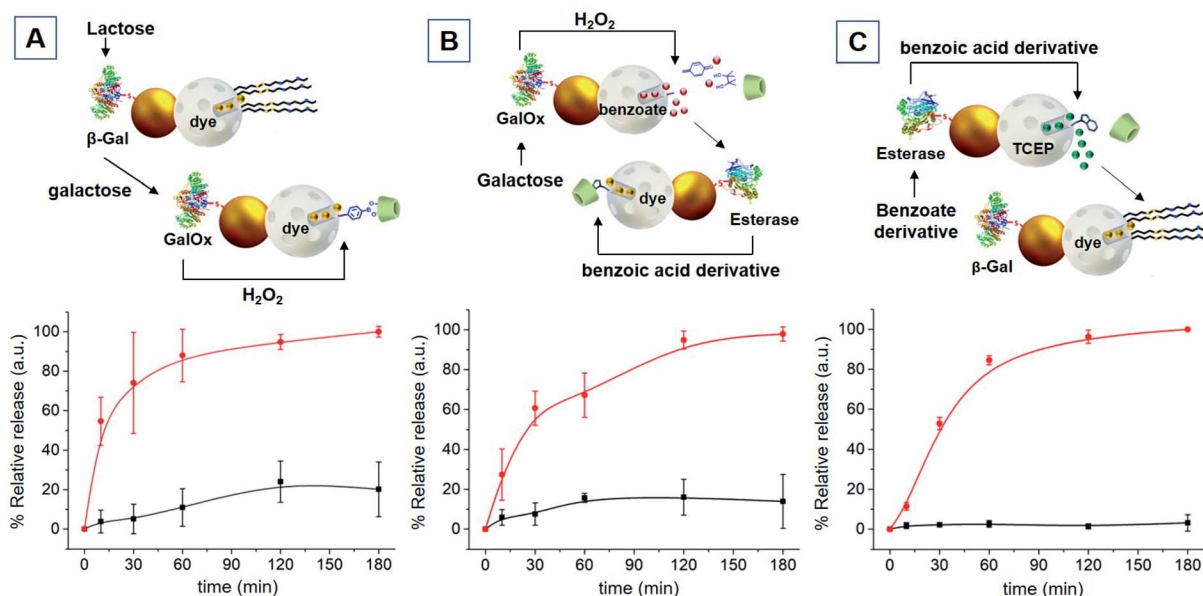


Fig. 4 Schemes of the experiments and normalized cargo release kinetics from each pair of nanoparticles (A) 1–2 ( $S1_{\beta gal}/S2_{gal ox}$ -dye), (B) 2–3 ( $S2_{gal ox}/S3_{est}$ -dye) and (C) 3–1 ( $S3_{est}/S1_{\beta gal}$ ) in the absence (black curves) and in the presence (red curves) of the corresponding input (lactose at 50 mM, galactose at 50 mM and methyl 4-(bromomethyl)benzoate at 1 mM final concentration, respectively). Error bars correspond to the s.d. from three independent experiments.



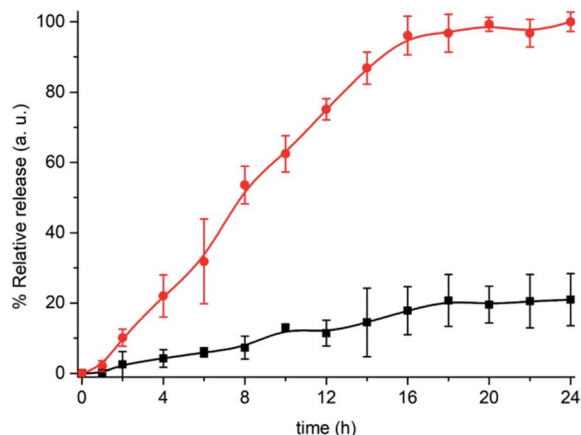


Fig. 5 Validation of the circular chemical communication network between the nanodevices 1, 2 and 3.  $[\text{Ru}(\text{bpy})_3]\text{Cl}_2$  release from  $\text{S1}_{\beta\text{gal}}$  in aqueous solution at pH 7.5 in the absence (black curve) and presence (red curve) of lactose (50 mM) in the complete community of nanoparticles ( $\text{S1}_{\beta\text{gal}}/\text{S2}_{\text{galox}}/\text{S3}_{\text{est}}$ ). Error bars correspond to the s.d. from three independent experiments.

continued sharply increasing until reaching saturation around 16 h. In our design, triggers that open the gating mechanism are orthogonal as the chemical messenger generated in the Au face only opens the gated mesoporous silica nanoparticle to which the Au unit is attached. In such a community of nanoparticles, release of the dye from  $\text{S1}_{\beta\text{gal}}$  after the addition of a stimulus (*i.e.* lactose) only becomes effective after the circular communication of the nanoparticles in the sequence  $\text{S1}_{\beta\text{gal}}-\text{S2}_{\text{galox}}-\text{S3}_{\text{est}}-\text{S1}_{\beta\text{gal}}$ .

When building cooperative networks of nanoparticles, it is crucial to understand each component's function and rule out potential side interactions and/or incompatibilities between the communities of nanodevices, resulting for instance in "unintended cross-talk" between nanodevices. In order to discard such effects, we performed additional delivery studies in the same conditions previously described using different combinations with "uncomplete" nanoparticles (*i.e.*, lacking either immobilized enzyme or cargo). As shown in Fig. 6, all combinations tested —  $\text{S1}/\text{S2}_{\text{galox}}/\text{S3}_{\text{est}}$  (lacking the enzyme on nanoparticle 1, bar B),  $\text{S1}_{\beta\text{gal}}/\text{S2}/\text{S3}_{\text{est}}$  (lacking the enzyme on nanoparticle 2, bar C),  $\text{S1}_{\beta\text{gal}}/\text{S2}_{\text{galox}}/\text{S3}$  (lacking the enzyme on nanoparticle 3, bar D),  $\text{S1}_{\beta\text{gal}}/\text{S2}_{\text{blank}}/\text{S3}_{\text{est}}$  (lacking the cargo in nanoparticle 2, bar E), and  $\text{S1}_{\beta\text{gal}}/\text{S2}_{\text{galox}}/\text{S3}_{\text{blank}}$  (lacking the cargo in nanoparticle 3, bar F) — showed much lower delivery in the presence of lactose compared to the complete community of nanoparticles ( $\text{S1}_{\beta\text{gal}}/\text{S2}_{\text{galox}}/\text{S3}_{\text{est}}$ , bar H). When one nanoparticle was not complete, the communication channel was disrupted and information was lost. In addition, we also studied the effect of having the enzymes in the solution instead of anchored to the nanoparticles. In a typical experiment the communities of nanoparticles  $\text{S1}/\text{S2}/\text{S3}$  (all lacking the enzyme) were brought in aqueous solution and enzymes at equivalent catalytic concentrations than in  $\text{S1}_{\beta\text{gal}}/\text{S2}_{\text{galox}}/\text{S3}_{\text{est}}$  were added to the mixture. As observed in Fig. 6 (bar G), the output signal (*i.e.*  $[\text{Ru}(\text{bpy})_3]\text{Cl}_2$  release) of the combination  $\text{S1}/\text{S2}/\text{S3}/\text{free}$

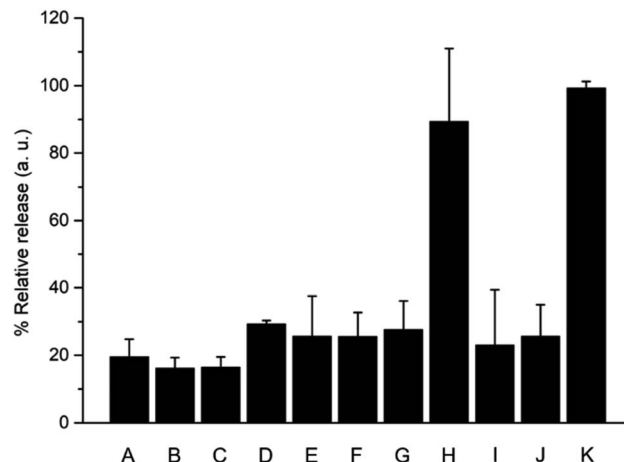


Fig. 6 Output signal from different partially-equipped communities of nanoparticles.  $[\text{Ru}(\text{bpy})_3]\text{Cl}_2$  release in aqueous solution at pH 7.5 in the presence of lactose (50 mM) containing the mixtures  $\text{S1}/\text{S2}_{\text{galox}}/\text{S3}_{\text{est}}$  (enzyme missing on nanoparticle 1, bar B),  $\text{S1}_{\beta\text{gal}}/\text{S2}/\text{S3}_{\text{est}}$  (enzyme missing on nanoparticle 2, bar C),  $\text{S1}_{\beta\text{gal}}/\text{S2}_{\text{galox}}/\text{S3}$  (enzyme missing on nanoparticle 3, bar D),  $\text{S1}_{\beta\text{gal}}/\text{S2}_{\text{blank}}/\text{S3}_{\text{est}}$  (cargo missing in nanoparticle 2, bar E),  $\text{S1}_{\beta\text{gal}}/\text{S2}_{\text{galox}}/\text{S3}_{\text{blank}}$  (cargo missing in nanoparticle 3, bar F),  $\text{S1}/\text{S2}/\text{S3}/\text{free}$  enzymes in bulk solution (bar G),  $\text{S1}/\text{S2}_{\text{galox}}/\text{S3}_{\text{est}}/\text{free}$   $\beta$ -galactosidase in bulk solution (bar H),  $\text{S1}_{\beta\text{gal}}/\text{S2}/\text{S3}_{\text{est}}/\text{free}$  galactose oxidase in bulk solution (bar I) and  $\text{S1}_{\beta\text{gal}}/\text{S2}_{\text{galox}}/\text{S3}/\text{free}$  esterase in bulk solution (bar J). Delivery from the full-equipped ( $\text{S1}_{\beta\text{gal}}/\text{S2}_{\text{galox}}/\text{S3}_{\text{est}}$ ) system in the absence (bar A) and the presence (bar K) of lactose (50 mM) is also displayed for comparative purposes. Communication was successfully achieved only when all components were present (bar K). Error bars correspond to the s.d. from three independent experiments.

enzymes was significantly lower compared to the response of the complete community which is ascribed to the dilution of the (free) enzyme-generated species in the solution. Moreover, the combinations  $\text{S1}_{\beta\text{gal}}/\text{S2}/\text{S3}_{\text{est}}/\text{free}$  galactose oxidase (bar I) and  $\text{S1}_{\beta\text{gal}}/\text{S2}_{\text{galox}}/\text{S3}/\text{free}$  esterase (bar J) at equivalent catalytic concentrations also showed a low delivery. These data demonstrate the importance of having the enzymes anchored to nanoparticles, which allows the generation of chemical micro-environments around the nanoparticles enabling the effective intracommunication between the enzyme on the Au face and silica gatekeepers as previously reported.<sup>25,31</sup> Furthermore, the mixture  $\text{S1}/\text{S2}_{\text{galox}}/\text{S3}_{\text{est}}/\text{free}$   $\beta$ -galactosidase (bar H) displayed a result comparable to the complete network; as  $\beta$ -galactosidase products act over a different nanoparticle (nanoparticle 2) the enzyme may or may not be attached to the nanoparticle 1 without disrupting the communication loop.

The behaviour of this circular model of communication between three nanodevices can be expressed in a Boolean logic table of 6 elements:<sup>39,40</sup> (*i.e.* the triggering species (lactose), enzyme  $\beta$ -galactosidase, enzyme galactose oxidase, cargo of nanoparticle 2 (methyl 4-(bromomethyl)benzoate), enzyme esterase and cargo of nanoparticle 3 (TCEP)). Among the 64 possible entries, only the combination of fully-equipped nanodevices  $\text{S1}_{\beta\text{gal}}/\text{S2}_{\text{galox}}/\text{S3}_{\text{est}}$  leads to a circular communication and efficient  $[\text{Ru}(\text{bpy})_3]\text{Cl}_2$  release (Tables S4 and S5 in ESI†).

**Efficiency studies.** Communication efficiency, process efficiency and information loss are relevant aspects that should be



considered when designing logic (chemical) communication systems. Three main processes/logical connections can be defined in our circular communication system: (i) connection 1–2 ( $S1_{\beta gal} - S2_{galox}$ ), (ii) connection 2–3 ( $S2_{galox} - S3_{est}$ ) and (iii) connection 3–1 ( $S3_{est} - S1_{\beta gal}$ ). Thus, the circular communication involves information transmission from one site to another in a hierarchical way following the order 1–2–3–1. In such a circuit, maximum communication efficiency would produce the maximum dye release from site 1. Accordingly, we evaluated the efficiency of the circular information transmission by comparing the output of the 1–2–3–1 process to the maximum possible output from site 1, and also determined the communication efficiency of sections of the circuit, *i.e.* pathway 2–3–1 and pathway 3–1 by external activation on site 2 and site 3, respectively (see Fig. 7A). For doing so, we ran delivery studies in parallel; (i) the dye-loaded nanoparticle  $S1_{\beta gal}$  with TCEP as input set the maximum output (cargo delivery) as 100% efficiency; (ii) measuring cargo delivery from  $S1_{\beta gal}$  in the  $S3_{est} - S1_{\beta gal}$  pair with methyl 4-(bromomethyl)benzoate as input allowed to calculate the 3–1 efficiency, (ii) whereas measuring cargo delivery from  $S1_{\beta gal}$  in the  $S2_{galox} - S3_{est} - S1_{\beta gal}$  system with galactose or lactose as inputs allowed calculation of the communication efficiency of the 2–3–1 and 1–2–3–1 processes, respectively. Cargo delivery from  $S1_{\beta gal}$  without input was set as the background release. From these communication efficiency data the efficiency for each 1–2, 2–3 and 3–1 communication step (process efficiency) was also calculated (Fig. 7B) (see ESI† for further information). For clarification, the different processes have been schematically represented in Fig. 7C. All the experiments were carried out with the same methodology, nanoparticle concentrations and input concentration (50 mM) than that followed in the experiment of Fig. 5 (details in ESI†). The results show that, as expected, the communication efficiency decreases by adding members (communications sites) and processes (connections) to the communication pathway resulting in certain chemical information loss (Fig. 7A and S15†). For instance, as depicted in Fig. 7A, dye delivery from 1 (*i.e.*  $S1_{\beta gal}$ ) in 3–1 reached maximum efficiency at 12 h whereas information transmission and delivery from 1 in the 2–3–1 section and the 1–2–3–1 circuit remain lower. In addition, at all times, communication efficiencies follow the tendency 3–1 > 2–3–1 > 1–2–3–1. In terms of information degradation after 24 h, no loss is observed for the shortest pathway (3–1) whereas it increases with the number of communication sites (members of the network), with 10% loss and 35% loss for 2–3–1 and 1–2–3–1 respectively (Fig. S15†). Information degradation within complex networks has been also observed by others both in solution and within immobilized communities.<sup>41,42</sup> Moreover, process efficiency (Fig. 7B) shows that process 1–2 quickly reaches values of *ca.* 60–70% and remains approximately constant with time. It can also be observed that the main rate limiting process in our system is the connection 2–3.

Altogether, the results described in this section illustrate how the analysis of process/communication efficiencies can help understand the complex behaviour of communication systems, identify critical steps, and facilitate the design of optimized networks. In addition, chemical communication networks could

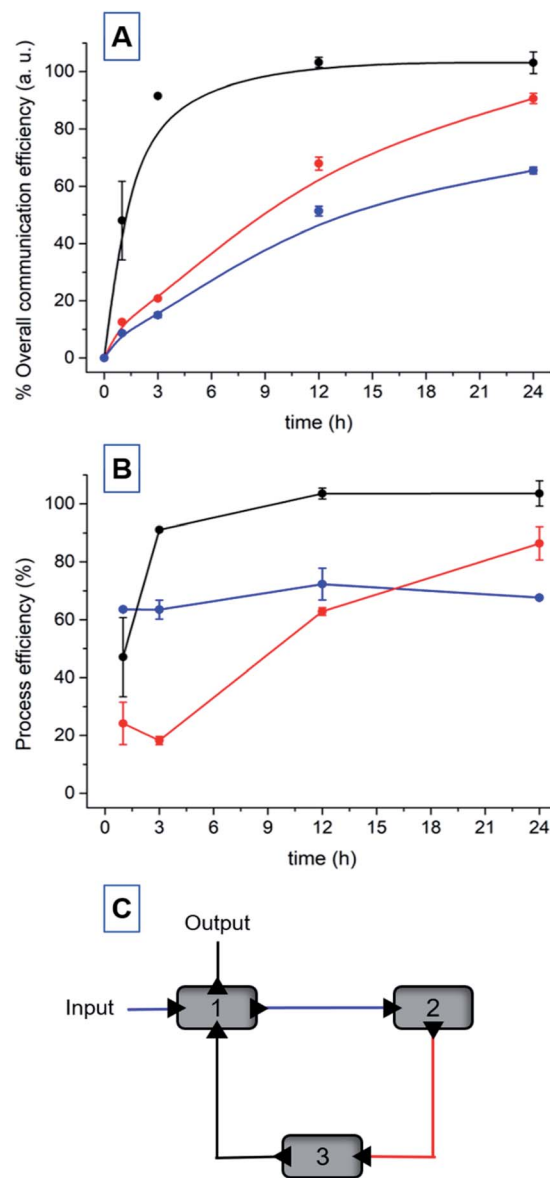


Fig. 7 (A) Overall communication (information transmission) efficiency for: circular sequence 1–2–3–1 ( $S1_{\beta gal} - S2_{galox} - S3_{est} - S1_{\beta gal}$ , blue curve), sequence 2–3–1 ( $S2_{galox} - S3_{est} - S1_{\beta gal}$ , red curve) and sequence 3–1 ( $S3_{est} - S1_{\beta gal}$ , black curve). (B) Process efficiency for the different connections of the circular communication system: 1–2 ( $S1_{\beta gal} - S2_{galox}$ , blue curve), 2–3 ( $S2_{galox} - S3_{es}$ , red curve), and 3–1 ( $S3_{est} - S1_{\beta gal}$ , black curve). Error bars in (A) and (B) correspond to the s.d. from two independent experiments. (C) General schematics of the communication system. Each coloured path corresponds to curves in (B).

be affected by spatial effects such as the relative distance between nanodevices/communication sites. Molecular messengers could be diluted in the medium before reaching its target,<sup>41</sup> directional information flow over distances in molecular communication circuits would require a fine control over the location of interacting nanodevices and messenger diffusion kinetics should be considered. In this study, we have conducted the experiments under stirring of solutions containing nanodevices; thus, diminishing the effect of particle location. Notwithstanding,

other works about chemical communication within communities of immobilized abiotic elements using microfluidic technologies have observed the importance of controlling geometrical patterning, chemical input concentrations and flow rate. Although so-far scarce, further studies in this direction will be important for advancing towards the design of chemical communication networks of nanodevices with spatiotemporal control over the information transmission.<sup>42,43</sup>

## Conclusions

In summary, we present herein a circular model of communication between nanodevices based on enzyme-functionalized Janus Au-mesoporous silica capped nanoparticles. In the community of nanoparticles, the release of a cargo from a first nanoparticle (output) after the addition of a stimulus (*i.e.* lactose) is only observed after the circular communication of the nanoparticles in the sequence  $S1_{\beta gal} \rightarrow S2_{galox} \rightarrow S3_{est} \rightarrow S1_{\beta gal}$  as a result of the exchange of chemical messengers between the components of the group. The relatively slow communication (maximum delivery after 16 h) is ascribed to the number of chemical processes that have to occur to communicate, including enzymatic activation of different molecules, cargo diffusion from the pores to the solution and chemical messenger diffusion from one nanoparticle to another. Moreover a calculation of the communication efficiency, process efficiency and information loss for the different steps of the communication path allowed us to better understand the communication network and determine the rate limiting processes. Several are the options to enhance communication; one of them is the use of nanoparticles equipped with nanomotors and several studies in this direction are being carried by us currently.<sup>44,45</sup> Overall, our network involves three enzymatic processes and the exchange of three chemical messengers (galactose, an ester derivative and the reducing agent TCEP). Only the complete community of nanoparticles is capable of producing the desired output phenomenon (dye release), while incomplete communities do not succeed in transmitting the information. In spite of being similar to a cascade-like system, its potential scope is beyond a typical metabolomic pathway because it is not only limited to the chained enzyme substrates and products. For instance, the possibility of encapsulating a cargo enables communication between enzymes that otherwise could not naturally interact. Moreover, nanoparticles can be directed, concentrated in certain places, *etc.*, allowing designing more advance communication systems, when compared with cascade-like system using chained enzymes in diluted solutions. Circular communication could be of relevance for designing networks enabling initiation of the communication and output from the same nanodevice after sequentially-programmed steps of information transmission with other nanodevices, thus potentially allowing feedback – this is an aspect that would not be possible with a linear pathway since signal detection and final response would occur on different sites. Although the presented design is a proof of concept which leads to a dye release as final output instead of the usual dynamical feedback observed in biological reaction cycles, it illustrates the potential of using abiotic nanodevices to design multistep signalling pathways. Our results

demonstrate how artificial nanodevices can be connected by means of molecular communication, yielding systems that show a collective synergic behaviour. Although modelling of the present system was beyond of our scope, advances in the modelling of molecular communications could help in the design and understanding of chemical networks at the micro/nanoscale. A search of different modes of communication within groups of nanoparticles (such as the circular mode of communication reported here) is a key step to further develop more realistic nano-communities to perform specific and complex tasks at the nanoscale. Moreover, the possibility of combining different nanoparticles and communicating them with living organisms<sup>46–49</sup> would allow to develop swarms of nanodevices able to interact with their neighbours and local environment leading to advanced systems with new cooperative functionalities. This would cause a deep impact in the way we understand the interaction between artificial nanodevices and nanodevices with living systems. We believe that the idea of developing multicomponent nanoscale cooperative communities capable of communicating and performing coordinated may open new directions in the near future in areas such as biomedicine and ICT.<sup>50–55</sup>

## Conflicts of interest

There are no conflicts to declare.

## Acknowledgements

The authors wish to thank the Spanish Government (projects RTI2018-100910-B-C41 (MCUI/AEI/FEDER, UE), CTQ2017-87954-P), the Generalitat Valenciana (PROMETEO 2018/024), the Comunidad de Madrid (IND2017/BMD-7642) and CIBERBBN (NANOCOMMUNITY project) for support.

## References

- 1 D. Malak and O. B. Akan, *Nano Commun. Netw.*, 2012, **3**, 19.
- 2 N. Deisig, F. Dupuy, S. Anton and M. Renou, *Insects*, 2014, **5**, 399.
- 3 M. E. Taga and B. L. Bassler, *Proc. Natl. Acad. Sci. U. S. A.*, 2003, **100**, 14549.
- 4 J. T. Hancock in *Cell Signalling*, Oxford University Press, Oxford, UK, 4th edn, 2016.
- 5 D. J. Levi in *Group Dynamics for Teams*, SAGE Publications, Thousand Oaks, CA, USA, 5th edn, 2016.
- 6 T. E. Harris and J. C. Sherblom in *Small Group and Team Communication*, Pearson, London, UK, 5th edn, 2010.
- 7 J. H. Miller and S. Moser, *Complexity*, 2004, **9**, 31.
- 8 R. E. Rice, E. J. Zackrisson and D. R. Seibold in *The International Encyclopedia of Organizational Communication*, John Wiley & Sons, NJ, USA, 1st edn, 2017.
- 9 P. F. Cristaldo, V. Jandák, K. Kutalová, V. B. Rodrigues, M. Brothánek, O. Jiríček, O. DeSouza and J. Sobotník, *Biol. Open*, 2015, **4**, 1649.





- 10 J. S. M. Chia, E. S. Wall, C. L. Wee, T. A. J. Rowland, R.-K. Cheng, K. Cheow, K. Guillemin and S. Jesuthasan, *Nat. Commun.*, 2019, **10**, 3831.
- 11 T. Eisner, I. Kriston and D. J. Aneshansley, *Behav. Ecol. Sociobiol.*, 1976, **1**, 83.
- 12 I. F. Akyildiz, F. Brunetti and C. Blázquez, *Comput. Netw.*, 2008, **52**, 2260.
- 13 J. L. Marzo, J. M. Jornet and M. Pierobon, *Curr. Drug Targets*, 2019, **20**, 800.
- 14 I. F. Akyildiz, M. Pierobon, S. Balasubramaniam and Y. Koucheryavy, *IEEE Commun. Mag.*, 2015, **53**, 32.
- 15 M. E. Roth, O. Green, S. Gnaim and D. Shabat, *Chem. Rev.*, 2016, **116**, 1309.
- 16 X. Sun, D. Shabat, S. T. Phillips and E. V. Anslyn, *J. Phys. Org. Chem.*, 2018, **31**, e3827.
- 17 S. Campuzano, B. Esteban-Fernandez de Ávila, P. Yáñez-Sedeño, J. M. Pingarrón and J. Wang, *Chem. Sci.*, 2017, **8**, 6750.
- 18 E. Aznar, M. Oroval, L. Pascual, J. R. Murguía, R. Martínez-Mañez and F. Sancenón, *Chem. Rev.*, 2016, **116**, 561.
- 19 C.-A. Cheng, T. Deng, F.-C. Lin, Y. Cai and J. I. Zink, *Theranostics*, 2019, **9**, 3341.
- 20 A. Llopis-Lorente, B. Lozano-Torres, A. Bernardos, R. Martínez-Mañez and F. Sancenón, *J. Mater. Chem. B*, 2017, **5**, 3069.
- 21 M. Karimi, A. Ghasemi, P. Sahandi Zangabad, R. Rahighi, S. Masoud Moosavi Basri, H. Mirshekari, M. Amiri, Z. Shafaei Pishabad, A. Aslani, M. Bozorgomid, D. Ghosh, A. Beyzavi, A. Vaseghi, A. R. Aref, L. Haghani, S. Bahramia and M. R. Hamblin, *Chem. Soc. Rev.*, 2016, **45**, 1457.
- 22 A. Llopis-Lorente, P. Díez, A. Sánchez, M. D. Marcos, F. Sancenón, P. Martínez-Ruiz, R. Villalonga and R. Martínez-Mañez, *Nano Today*, 2018, **18**, 8.
- 23 H. Wang and M. Pumera, *Chem. Soc. Rev.*, 2020, **49**, 3211.
- 24 C. Giménez, E. Climent, E. Aznar, R. Martínez-Mañez, F. Sancenón, M. D. Marcos, P. Amorós and K. Rurack, *Angew. Chem., Int. Ed.*, 2014, **53**, 12629; *Angew. Chem.*, 2014, **126**, 12838.
- 25 A. Llopis-Lorente, P. Díez, A. Sánchez, M. D. Marcos, F. Sancenón, P. Martínez-Ruiz, R. Villalonga and R. Martínez-Mañez, *Nat. Commun.*, 2017, **8**, 15511.
- 26 C. Chen, X. Chang, H. Teymourian, D. E. Ramírez-Herrera, B. Esteban-Fernández de Ávila, X. Lu, J. Li, S. He, C. Fang, Y. Liang, F. Mou, J. Guan and J. Wang, *Angew. Chem., Int. Ed.*, 2018, **57**, 241; *Angew. Chem.*, 2018, **130**, 247.
- 27 Y. Qiao, M. Li, D. Qiu and S. Mann, *Angew. Chem., Int. Ed.*, 2019, **58**, 17758; *Angew. Chem.*, 2019, **131**, 17922.
- 28 T. Farrugia, A. W. Perriman, K. P. Sharma and S. Mann, *Chem. Commun.*, 2017, **53**, 2094.
- 29 W. Wang, W. Duan, S. Ahmed, A. Sen and T. Mallouk, *Acc. Chem. Res.*, 2015, **48**, 1938.
- 30 W. Bechtel and A. Abrahamsen in *Philosophy of Complex Systems*, Elsevier, Amsterdam, Netherlands, 1st edn, 2011, Part 2, Ch. 1.
- 31 R. Villalonga, P. Díez, A. Sánchez, E. Aznar, R. Martínez-Mañez and J. M. Pingarrón, *Chem.-Eur. J.*, 2013, **19**, 7889.
- 32 A. Llopis-Lorente, B. de Luis, A. García-Fernández, P. Díez, A. Sánchez, M. D. Marcos, R. Villalonga, R. Martínez-Mañez and F. Sancenón, *J. Mater. Chem. B*, 2017, **5**, 6734.
- 33 T. M. Godoy-Reyes, A. Llopis-Lorente, A. García-Fernández, P. Gaviña, A. M. Costero, R. Villalonga, F. Sancenón and R. Martínez-Mañez, *Org. Chem. Front.*, 2019, **6**, 1058.
- 34 F. O. Yousef, M. B. Zughul and A. A. Badwan, *J. Inclusion Phenom. Macrocyclic Chem.*, 2007, **57**, 519.
- 35 G. Jerez, G. Kaufman, M. Prystai, S. Schenkeveld and K. K. Donkor, *J. Sep. Sci.*, 2009, **32**, 1087.
- 36 S. S. Wong and L.-J. C. Wong, *Enzyme Microb. Technol.*, 1992, **14**, 866.
- 37 A. Kasprzak, K. M. Borys, S. Molchanov and A. Adamczyk-Wozniak, *Carbohydr. Polym.*, 2018, **198**, 294.
- 38 A. Llopis-Lorente, B. de Luis, A. García-Fernández, S. Jiménez-Falcao, M. Orzáez, F. Sancenón, R. Villalonga and R. Martínez-Mañez, *ACS Appl. Mater. Interfaces*, 2018, **10**, 26494.
- 39 S. Erbas-Cakmak, S. Kolemen, A. C. Sedgwick, T. Gunnlaugsson, T. D. James, J. Yoon and E. U. Akkaya, *Chem. Soc. Rev.*, 2018, **47**, 2228.
- 40 *Biomolecular Information Processing: From Logic Systems to Smart Sensors and Actuators*, ed. E. Katz, John Wiley & Sons, 1st edn, NJ, USA, 2012.
- 41 G. Gines, A. S. Zadorin, J.-C. Galas, T. Fujii, A. Estevez-Torres and Y. Rondelez, *Nat. Nanotechnol.*, 2017, **12**, 351.
- 42 L. Tian, M. Li, J. Liu, A. J. Patil, B. W. Drinkwater and S. Mann, *ACS Cent. Sci.*, 2018, **4**, 1551.
- 43 J. Liu, L. Tian, Y. Qiao, S. Zhou, A. J. Patil, K. Wang, M. Li and S. Mann, *Angew. Chem., Int. Ed.*, 2020, **59**, 6853.
- 44 A. Llopis-Lorente, A. García-Fernández, E. Lucena-Sánchez, P. Díez, F. Sancenón, R. Villalonga, D. A. Wilson and R. Martínez-Mañez, *Chem. Commun.*, 2019, **55**, 13164.
- 45 A. Llopis-Lorente, A. García-Fernández, N. Murillo-Cremaes, A. C. Hortelão, T. Patiño, R. Villalonga, F. Sancenón, R. Martínez-Mañez and S. Sánchez, *ACS Nano*, 2019, **13**, 12171.
- 46 R. Lentini, N. Y. Martin, M. Forlin, L. Belmonte, J. Fontana, M. Cornella, L. Martini, S. Tamburini, W. E. Bentley, O. Jousson and S. S. Mansy, *ACS Cent. Sci.*, 2017, **3**, 117.
- 47 B. de Luis, A. Llopis-Lorente, P. Rincón, J. Gadea, F. Sancenón, E. Aznar, R. Villalonga, J. R. Murguía and R. Martínez-Mañez, *Angew. Chem. Int. Ed.*, 2019, **58**, 14986; *Angew. Chem.*, 2019, **131**, 15128.
- 48 C. G. Hebert, A. Gupta, R. Fernandes, C. Y. Tsao, J. J. Valdes and W. E. Bentley, *ACS Nano*, 2010, **4**, 6923.
- 49 M. Schwarz-Schilling, L. Aufinger, A. Mückl and F. C. Simmel, *Integr. Biol.*, 2016, **8**, 564.
- 50 S. Hauert and S. N. Bhatia, *Trends Biotechnol.*, 2014, **32**, 448.
- 51 N. Agoulmine, K. Kim, S. Kim, T. Rim, J.-S. Lee and M. Meyyappan, *IEEE Wirel. Commun.*, 2012, **19**, 42.
- 52 N. Farsad, *Mob. Comput. Commun. Rev.*, 2018, **22**, 5.
- 53 T. Nakano, M. J. Moore, F. Wei, A. V. Vasilakos and J. Shuai, *IEEE Trans. Nanobioscience*, 2012, **11**, 135.
- 54 A. García-Fernández, E. Aznar, R. Martínez-Mañez and F. Sancenón, *Small*, 2020, **16**, 1902242.
- 55 O. B. Akan, H. Ramezani, T. Khan, N. A. Abbasi and M. Kescu, *Proc. IEEE*, 2017, **105**, 306.

